ELSEVIER

Journal of Structural Geology 26 (2004) 905–917

JOURNAL OF STRUCTURAL GEOLOGY

www.elsevier.com/locate/jsg

The effect of non-parallel thrust fault interaction on fold patterns

Heather M. Savage*, Michele L. Cooke

Geosciences Department, University of Massachusetts Amherst, 611 North Pleasant St., Amherst, MA 01003, USA

Received 18 September 2002; received in revised form 12 August 2003; accepted 12 September 2003

Abstract

The geometry of two subsurface non-parallel thrust faults are systematically altered within mechanical models to determine the range of resulting fold map patterns and the effect of fault interaction on these fold patterns, and ultimately to infer fault geometry from complex fold shapes. Multiple faults can create both complex fold patterns with more than one fold axis and single folds without evidence of a second fault. Fold length may not correlate to fault length when remote contraction is oblique to the faults; thus contraction direction should be determined before fault length is inferred. The influence of fault interaction is studied by comparing the fold pattern created by interacting faults to the fold pattern created from the superposition of folds produced by equivalent but isolated faults. Under small strains, larger faults tend to have greater interaction but even interacting faults may not produce fold patterns notably distinct from the superposed fold patterns. This suggests that fault interaction need not necessarily be considered when inferring fault geometry from fold shape in the field; however, under non-coaxial strain conditions fold patterns may differ from those presented here.

Keywords: Thrust fault interaction; Fold pattern; Fault geometry; Sheep Mountain Anticline

1. Introduction

Where faults do not reach the Earth's surface, the only surface evidence of the presence and geometry of underlying faults may be fold patterns. Fault geometry has been inferred from fold shapes observed in the field (e.g. Shamir and Eyal, 1995; Rowan and Linares, 2000) and from seismic data (e.g. Allmendinger and Shaw, 2000). Model results aid this inference by demonstrating that the shape of isolated folds can be directly linked to the geometry of underlying faults (e.g. Suppe, 1983; Suppe and Medwedeff, 1990; Cooke and Pollard, 1997; Johnson and Johnson, 2001; Savage and Cooke, 2003). However, faults seldom occur in isolation and the fold patterns created from multiple faults can be complex, with multiple or branching fold axes. Deciphering fault geometries from intricate fold patterns is not straightforward. Although Shamir and Eyal (1995) inferred the geometry of multiple faults from observed fold patterns by considering isolated faults, the influence of fault interaction on suprajacent fold patterns has yet to be investigated. In order to infer critical aspects of fault geometry from complex fold patterns, it is necessary first to understand the range of fold patterns produced by variations in a simple system of two interacting faults. Fold pattern may be influenced by both changes to the fault geometry and changes to the orientation of each fault with respect to the principal contraction direction. For example, faults striking oblique to the maximum contraction direction have been shown to have oblique slip and produce asymmetric fold shapes in areas of anisotropic rock (Smith and Marshall, 1992).

Studies have shown that fault interaction redistributes slip (e.g. Willemse et al., 1996; Maerten et al., 1999), which may alter the overlying folds so that the pattern is not equivalent to superposing folds associated with isolated faults of equivalent geometry. Furthermore, slip distribution can serve as an indicator of the degree of fault interaction; the slip distribution for parallel (Willemse et al., 1996) and non-parallel (Maerten et al., 1999) interacting faults both differ significantly from slip distribution on an isolated fault. Willemse et al. (1996) show that slip is greatest at overlaps for parallel échelon faults and Maerten et al. (1999) found intersecting normal faults to have the greatest slip at the intersection. Furthermore, Cashman and Ellis (1994) demonstrated that rupture events on nearby faults could

* Corresponding author. Present address: Department of Geosciences, The Pennsylvania State University, University Park, PA 16802, USA. Tel.: +1-814-865-9353; fax: +1-413-545-1200.
E-mail address: hsavage@geosc.psu (H.M. Savage).

0191-8141/$ - see front matter © 2004 Elsevier Ltd. All rights reserved.
doi:10.1016/j.jsg.2003.09.006

cause up to five different directions of slickenlines along one fault without changing the remote stress field; thus the presence of nearby faults can influence the slip pattern.

Motivated by the complex fold pattern at Sheep Mountain Anticline, Wyoming, a Laramide-age doubly plunging anticline, this study investigates the production of multiple fold patterns and what effect, if any, fault interaction has on fold pattern. Sheep Mountain Anticline is located in the foreland of the Rocky Mountains within the northern Big Horn Basin, Wyoming (Fig. 1).

We also determine whether geometry of the subsurface faults can be resolved from analysis of associated fold patterns. For this study, three aspects of fold pattern and interaction are explored. First, we analyze the range of fold patterns resulting from a suite of two-fault models that systematically varies the geometry of one fault. Second, we test the influence of fault interaction on fold pattern by comparing a fold pattern created from two interacting faults with a pattern produced from superposition of folds created by equivalent but isolated faults. Differences between this superposed fold pattern and the interactive pattern highlight the contribution of fault interaction to folding. Finally, for models that show a significant difference between isolated and interacting fold patterns, fault slip is mapped to determine how much interaction is needed to significantly change fold pattern.

2. Methods and model set-up

A sensitivity analysis is conducted to constrain the array of fold shapes produced by two faults in one episode of contraction. We create models using the boundary element method code, *Poly3D*, which solves the governing equations of continuum mechanics for an angular dislocation in an elastic half-space (Thomas, 1994). The boundary element method calculates the stress and displacements within a linear-elastic body after tractions or displacements have been applied to the boundaries (Crouch and Starfield, 1990). A system of linear equations can determine the displacement and stress at any point caused by the far field and boundary conditions; in this model the boundaries are the fault planes. By discretizing only the fault surfaces, this tool is more efficient than the finite element method codes that require greater computation for similar results (Crouch and Starfield, 1990).

To simulate linear elastic deformation of a moderately stiff sandstone, a Poisson's ratio of 0.25 and a shear modulus of 12,000 MPa are prescribed. A remote contraction of 1% is applied to each model to promote slip along, and interaction between, the faults and create folds at the model surface. Faults are introduced into the model as static (non-propagating) elliptical discontinuities. The faults are freely-slipping, not permitted to open or overlap and have an

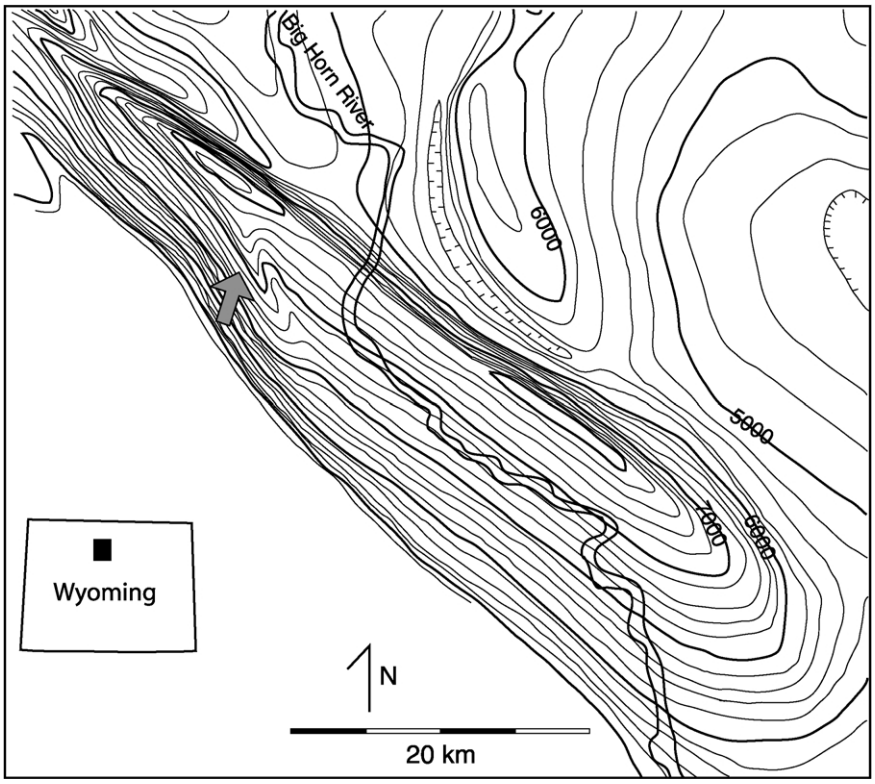

Fig. 1. Structure contour map of Sheep Mountain Anticline (taken from Andrews et al., 1944). Gray arrow points to small secondary fold off the southwestern flank of the anticline. Contour interval is 200 feet. The secondary fold has been interpreted to overly a splay fault that branches from the major fault underlying Sheep Mountain Anticline (Hennier and Spang, 1983).

aspect ratio of 2:1 (length:height). The geometry of the longer, primary fault is held constant throughout the experiment (Fig. 2). The secondary, smaller fault is systematically varied in size, dip and depth along with distance from and orientation to the primary fault (Fig. 2). Additionally, strain direction is varied in some models.

3. Fold patterns

Investigation into the surface fold pattern for each suite of interacting faults reveals that significant changes in fold pattern can occur with minor changes in fault parameters. For the purpose of this discussion, a pattern with more than one discernible fold axis including any type of splay or perturbation from a single fold shape is considered a multiple fold pattern. The two-fault model can produce both multiple fold patterns and patterns negligibly different from the fold shape produced by the isolated primary fault.

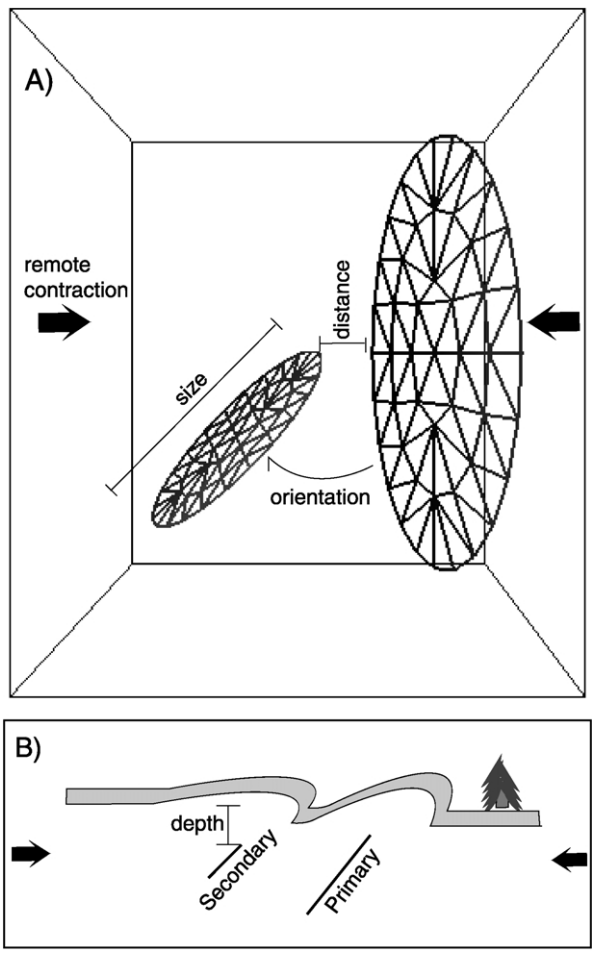

Fig. 2. Model set-up. The geometry of the primary fault is held constant at 10 km length, 1 km depth with an aspect ratio of 2:1 (length:height) and dipping 60° to the west. The secondary fault varies in size, depth, and dip along with distance from and orientation to the primary fault.

3.1. Depth and size of secondary fault

The effects of depth and size of the secondary fault are considered together because their results are interrelated (i.e. larger and shallower secondary faults produce greater folding than deeper or smaller faults). Secondary faults cannot create a distinctive secondary fold if buried deeper than the primary fault (Fig. 3, right column), unless the fault size exceeds approx. 50% of the primary fault (Fig. 3I). With faults at equal depth (Fig. 3, middle column), secondary faults as small as 30% the size of the primary fault produce secondary folds (Fig. 3E and H). Secondary faults shallower than primary faults create a secondary fold if they exceed 10% of the size of the primary fault (Fig. 3, left column).

Slip along small and deep secondary faults does not seem to contribute to the fold pattern (Fig. 3A–C and F). Under these conditions the deformation associated with the primary fault greatly exceeds that of the secondary fault so that contributions of the secondary fault to folding are overwhelmed. However, when the secondary fault is shallower than the primary fault, the secondary fault-tip stress field emerges from the shadow of the primary fault and produces a secondary fold. Furthermore, when the secondary fault is shallower, the fault has thinner suprajacent material, which creates less resistance to folding, and results in greater fold amplitude.

3.2. Secondary fault dip

Fault dip plays a smaller role in creating a distinct secondary fold than the other parameters investigated because, unless the fault dips horizontally, remote contraction drives slip on the secondary fault, producing associated folding (Fig 4). However, fold pattern changes with fault dip. A fault dip of 45° creates the most distinct fold; secondary folds become less distinct with greater or lesser dip. The 45° dipping fault accommodates greatest deformation because it is aligned with the plane of maximum shear stress under horizontal contraction. Under conditions of frictional fault slip, a shallower fault dip would be preferred. The vertical secondary fault experiences significant strike-slip that shifts the secondary anticline axis further north and to an east–west trend (Fig. 4A).

3.3. Secondary fault strike

Secondary fault strike greatly influences the development of secondary folds. The most distinct secondary fold arises where the secondary fault trends sub-parallel to the primary fault (Fig. 5), as this orientation, nearest to perpendicular to the remote contraction, is the most favored for dip-slip. A secondary fault strike of 020° (Fig. 5C) creates a taller and longer secondary fold than a fault trending 045° (Fig. 5B). When the secondary fault parallels

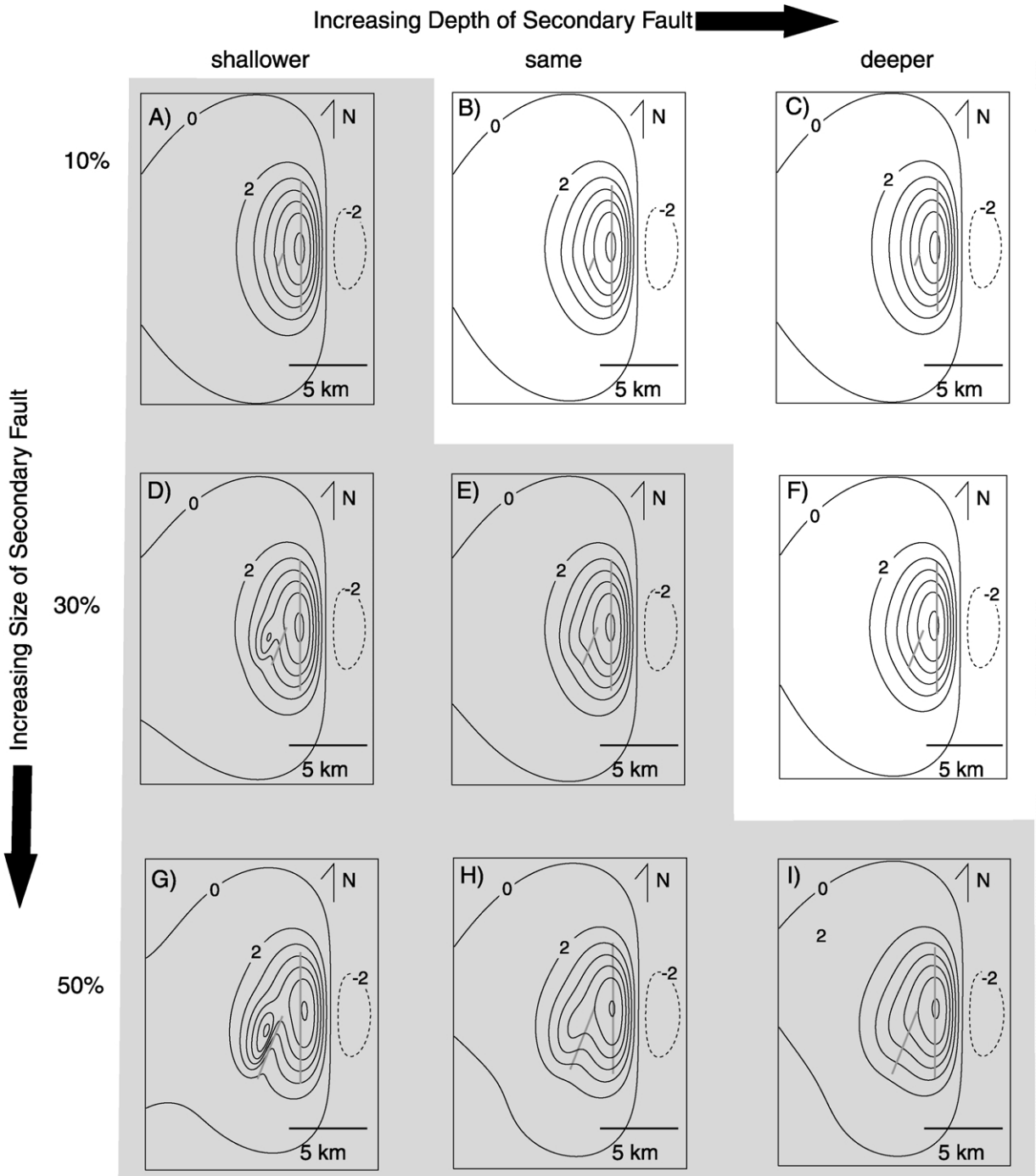

Fig. 3. Surface fold patterns for secondary faults at depths of 0.25 km (left column), 1 km (center column) and 0.75 km (right column). Sizes of secondary faults increase from 1 km (top row) to 3 km (center row) to 5 km (bottom row). Thick gray lines in this and subsequent figures show traces of the upper tip of the faults. Contour interval is 2 m. The dip and orientation of the secondary faults are held constant at 60° and 20°, respectively. The gray box outlines the multiple fold patterns whereas folds outside the gray box resemble isolated folds. The pattern in (A) contains slight perturbation from an isolated fold pattern along the left limb.

the contraction direction (Fig. 5A), no slip occurs along the fault and no secondary fold forms.

3.4. Remote contraction direction

Just as the secondary fold changes at different fault strikes, so will the overall pattern change with a change in the remote contraction direction. Contraction directions of 045° and 135° produce greater strike-slip along the main fault than 090° contraction directions (Fig. 6). This strike-slip along the primary fault produces a suprajacent fold with one of the fold terminations tighter than the other

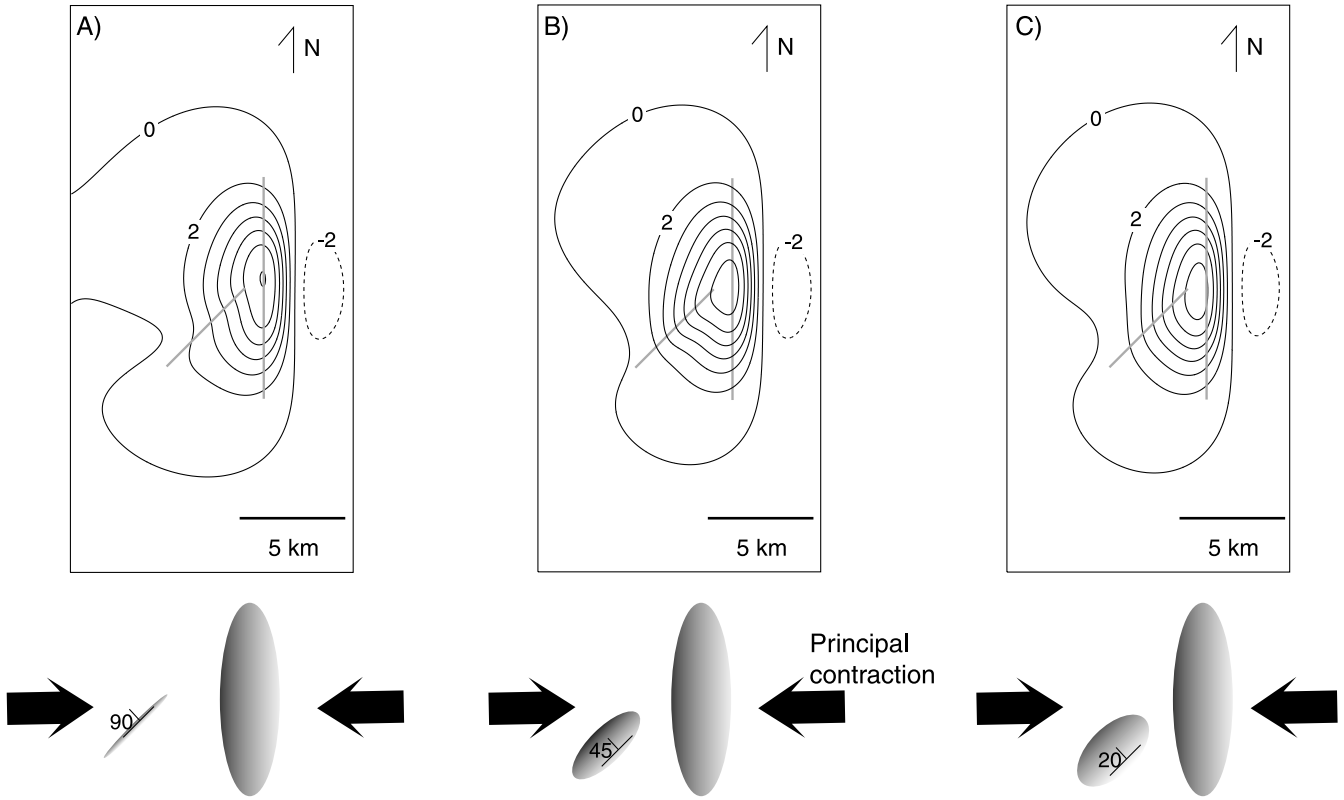

Fig. 4. Surface fold patterns for (A) 90°, (B) 45° and (C) 20° dipping secondary fault. Contour interval is 2 m. Secondary fold becomes less distinct at dips greater or lesser than 45°.

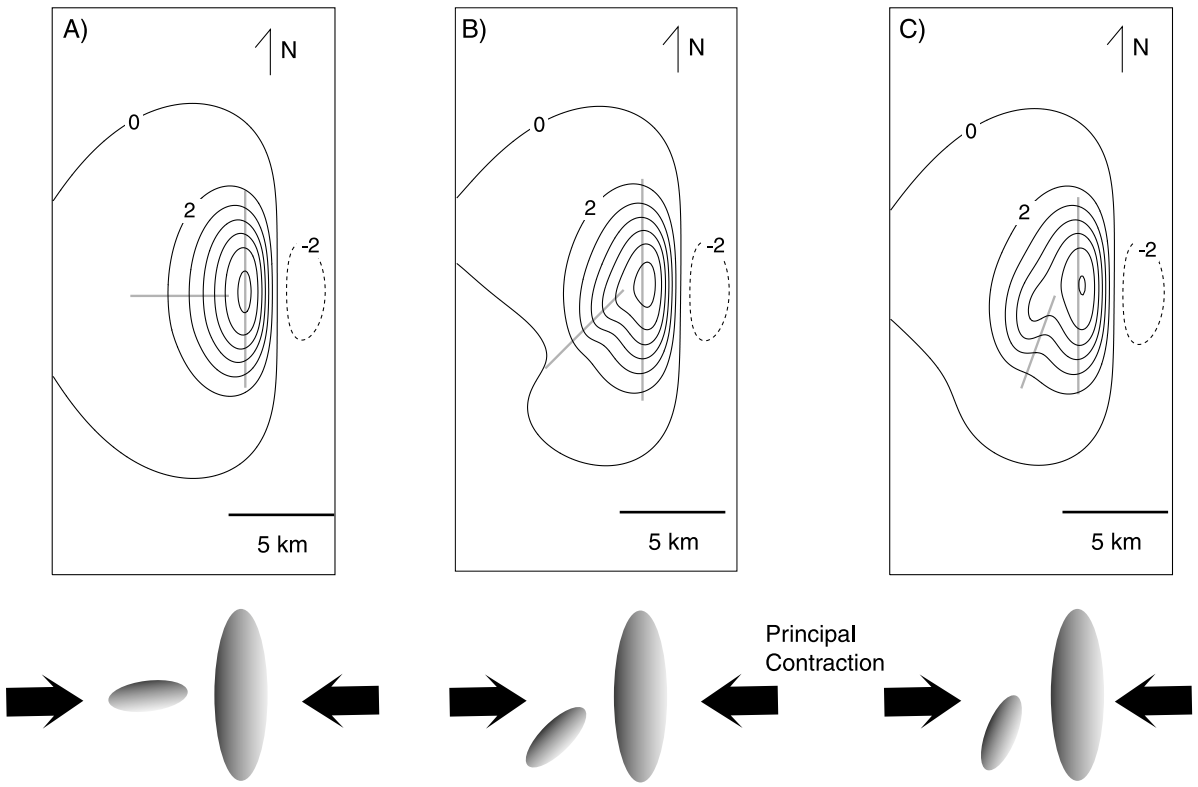

Fig. 5. Surface fold patterns as the strike of the secondary fault varies from (A) 090° to (B) 045° to (C) 020°. Contour interval is 2 m. The most distinct secondary fold is created as the secondary fault strikes nearly perpendicular to the remote contraction direction and sub-parallel to the primary fault.

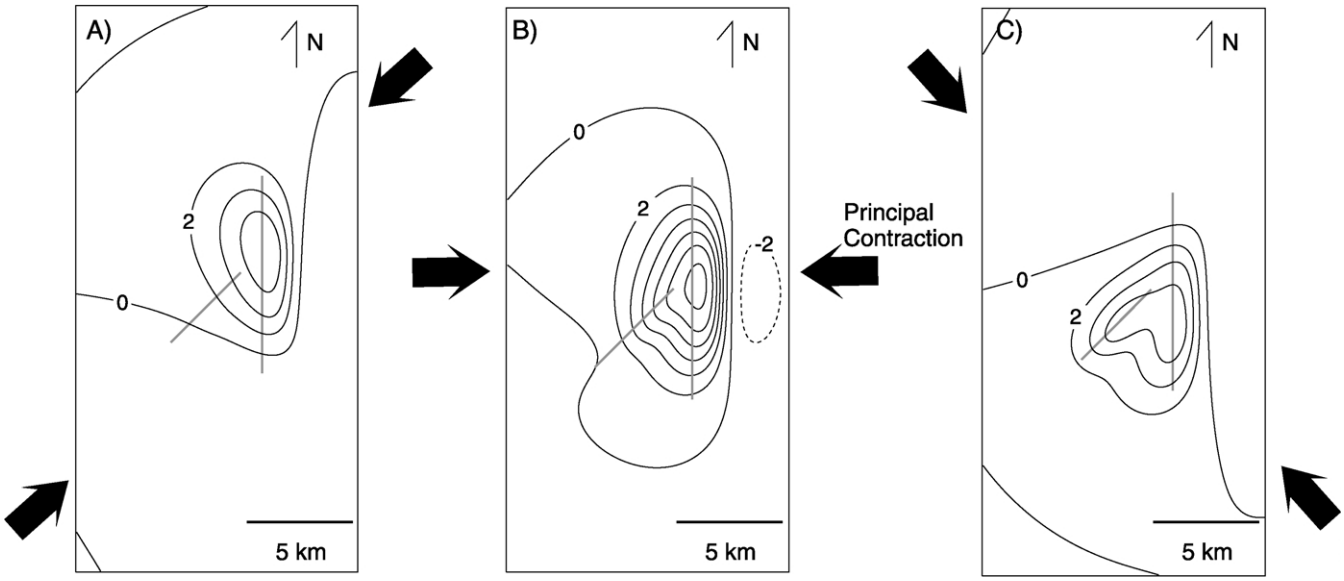

Fig. 6. Surface fold pattern for principal contraction directions of (A) 045°, (B) 090° and (C) 135°. Secondary fault configuration is held constant at 045° strike, 60° dip and a length of 5 km. Contour interval is 2 m. Contraction oblique to the primary fault promotes strike-slip, which creates asymmetry to the primary fold terminations. The fold pattern of (C) suggests two equal-sized faults but was created by applying contraction perpendicular to the smaller fault.

(e.g. Fig. 6A). A 045° contraction direction, parallel to the secondary fault, produces no splay fold (Fig. 6A) because the secondary fault cannot slip. In contrast, when the contraction is perpendicular to the secondary fault, increased dip-slip on the secondary fault creates a secondary fold as large as the primary fold (Fig. 6C), even though the secondary fault is half the size of the primary fault.

The model results indicate that relative fold length cannot be used to determine fault length without constraints on the remote contraction direction. For example, without knowing fault size, the fold pattern of Fig. 6C might suggest approximate equally-sized faults. However, fold characteristics may be helpful in determining the relative orientation of the fault to contraction direction. For example, faults that strike oblique to the principal contraction direction produce asymmetrically terminated folds (Fig. 6A).

3.5. Separation between faults

The fold patterns for two different sizes of secondary faults (50 and 100% primary fault length) are explored for three different distances, specifically: separated (1 km between the tip of the secondary fault and the primary fault; Fig. 7A and D), connected (the tip of the secondary fault and the center of the main fault share a vertex; Fig. 7B and E) and mated (the secondary fault is a half ellipse abutting against the primary fault; Fig. 7C and F). The separated and connected models have identical fault geometry except for the distance of separation. For the mated model, the secondary fault length remains the same as the other models but the shape is a half-ellipse to allow full intersection with the primary fault.

In agreement with the results of Section 3.1 (Fig. 3) all models with same length secondary and primary faults produce distinct secondary folds (Fig. 7A–C). The connected faults produce a narrower overall fold pattern with a slightly steeper secondary forelimb (Fig. 7B) than the separated faults (Fig. 7A); however, the fold patterns do not differ greatly. The mated equal-length faults produce fold shapes resembling that of connected faults except for a bulge on the eastern limb of the primary fold where the two faults intersect (Fig. 7C).

Shorter secondary faults only create secondary folds when separated or connected to the primary fault (Fig. 7D and E); however, the secondary fold is faint when the two faults touch. The mated faults produce a fold closely resembling that produced by an isolated primary fault (Fig. 7F).

3.6. Implications of secondary fault sensitivity analysis

Because not all configurations of multiple faults produce multiple folds, the presence of a multiple fold pattern partially constrains the fault geometry. Either the faults must be similar in size and of a similar depth, or else the smaller fault must be shallower than the larger fault. Additionally, neither fault can parallel the maximum contraction direction. Contraction perpendicular to the secondary fault creates a large secondary fold, even if the fault is much smaller than the primary fault. This result has significant implications for the inference of coeval non-parallel faults where both faults cannot be perpendicular to the contraction direction at the same time. Because fold length does not correlate to fault length when faults undergo oblique slip, contraction direction must be approximated before fault size can be inferred from fold patterns. Folds terminations of differing tightness may indicate oblique fault slip and assist in deducing contraction direction.

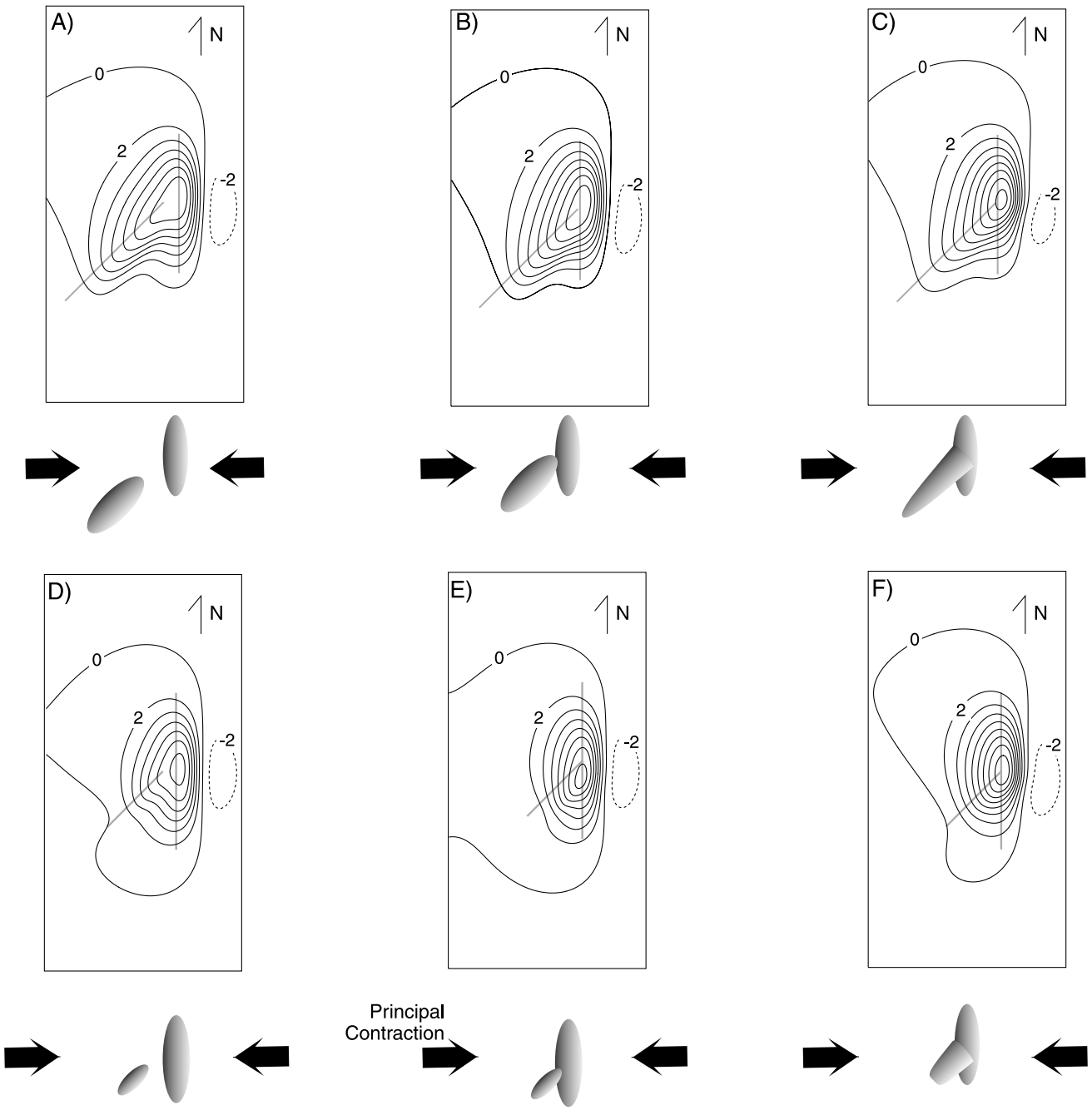

Fig. 7. Surface fold pattern as distance between the faults decreases from 1 km (left column) to touching, where faults share one vertex (center column) and mated, where the two faults share several vertices (right column). The secondary fault in the first row is 10 km long, dips 60° and strikes 045°. In the second row the secondary fault is 5 km long, dips 60° and strikes 045°. Contour interval is 2 m. The fold pattern of (F) shows no evidence of a second fault.

Generally, intersecting faults of equal depth can create a single fold if the secondary fault is 50% the length of the primary and intersecting faults create multiple folds if the secondary fault is longer than 50% the length of the primary. Although faults less than 50% the length of the primary can create secondary folds when the two faults are separated, folding associated with the secondary fault becomes overwhelmed along more proximal faults. These results suggest that multiple faults can be present in the subsurface but either the dominance of larger faults or strike of faults relative to the principal contraction inhibits expression of multiple surface folds. In active tectonic environments these unrecognized faults could be activated if a local change in the stress field caused the secondary fault to become less favorably aligned for slip, thereby allowing the inactive part of the primary fault to emerge from its shadow.

3.7. Application to Sheep Mountain Anticline, Wyoming

Using Sheep Mountain Anticline and its splay fold again

as an example, some elements of the subsurface fault geometry can be estimated based on the similarity of the exposed fold pattern to modeled fold patterns For instance, Sheep Mountain Anticline appears roughly symmetrically terminated (Fig. 1) indicating that the remote contraction direction was most likely nearly perpendicular to the fold. In contrast, remote contraction direction oblique to the larger fault produces a nearly triangular fold (Fig. 6A). The size of the Sheep Mountain splay fold resembles Fig. 3D, indicating that the splay may be approximately 30% the length of the Sheep Mountain fault and at a shallower depth. Comparison of the shape of the splay fold with Fig. 4 suggests that the secondary fault is most likely dipping around 45° or steeper but not as steep as 90°. The trend of the secondary fold axis suggests that the splay fault may strike around 20° from the main fault (e.g. Fig. 5). Because we have already inferred from the secondary fold length that the secondary fault is less than 50% the length of the main fault, comparison of fold shape with the separation analysis presented in Fig. 7 suggests that the faults are not likely connected. Together, these inferences from fold patterns constrain many aspects of subsurface fault geometry at Sheep Mountain Anticline. Our inferred geometry can be compared with the results of Hennier and Spang's (1983) geometric structural analysis. They estimate that the splay fault dips 45–80°, which overlaps with the range we infer from the map fold pattern. Unlike our study, the structural cross-sections indicate that the splay and primary fault connect at depth although such intersection may not be conclusive from the structural analysis. The analysis of subsurface fault geometry is useful for understanding fault connectivity and subsequent implications for fluid flow because faults can act as either seals or conduits for fluid flow. By using observed fold patterns, some aspects of fault geometry might be outlined more quickly than a full-scale structural analysis.

4. Fault interaction and fold patterns

Previous studies of fault interaction have focused on the redistribution of slip (e.g. Willemse et al., 1996; Maerten et al., 1999), which can result in phenomena such as earthquake triggering (e.g. Mikumo et al., 1999), but the effects of fault interaction on fold pattern are not well known. For all of the models presented here, faults are allowed to interact because we do not constrain slip along the faults; subsequently, this interaction may influence the resultant fold patterns presented in Section 3. To assess the role of fault interaction on fold pattern, the second part of this paper compares superposed folds created by isolated faults to fold patterns created by interacting faults. The difference between the two patterns may reflect the difference between coeval and successive folding. Furthermore, the results of comparing fold patterns will guide the inference of fault geometry from multiple fold patterns by delineating conditions where fault interaction need not be considered in analysis of fold patterns. Under such conditions, the geometry of each unexposed fault can be independently assessed from each exposed fold so that coeval non-parallel folding can be considered similar to successive folding. However, if fault interaction significantly alters the resulting fold pattern, the fault geometry inferred from individual fold shapes may err.

For each fault pair from the sensitivity analysis, the fold pattern created by an interacting fault pair is compared with a fold pattern created by superimposing folds formed by isolated primary and secondary faults (Fig. 8). Because we use infinitesimal strains, linear elasticity is assured and the fold shapes can be summed without concern regarding order of deformation. The identical fault geometry is used in both the interactive and superposed models and the difference between the interactive and superposed fold patterns shows the degree to which fault interaction contributes to folding. Positive fold amplitude difference indicates the interactive model has greater folding while negative difference indicates the superposed model has greater folding (Fig. 8).

5. Results of fault interaction analysis

To explore the contribution of fault interaction to fold pattern, each fault system is considered to have either negligible interaction or some degree of interaction based on the maximum percent difference in uplift between the interactive and isolated fold surfaces (Table 1). Because we expect relative fault size and proximity to have the greatest influence on fault interaction, the change in fold pattern reported in Table 1 is based on the fault configurations shown in Fig. 7. Configurations with $<5\%$ uplift difference are considered to have negligible fault interaction because the changes in fold pattern are minimal, whereas in configurations with greater than 5% uplift difference, fault interaction visibly alters the fold pattern. A 5–10% uplift difference reflects moderate changes to fold amplitude; however, the overall fold pattern remains the same. Models with greater than 10% change in uplift have slight changes to the fold pattern.

5.1. Fault configurations with negligible interaction (maximum Δ in uplift $<5\%$)

Configurations with small secondary faults and great

Table 1
Maximum percent uplift difference of folded surfaces for interacting and superposed models

Size of secondary fault	Separated 1 km apart	Connected 0 km apart	Mated 0 km apart
50% of primary	1%	1.5%	14%
100% of primary	8%	12%	26%

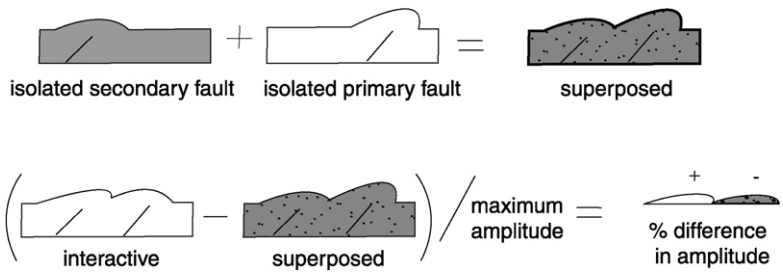

Fig. 8. Percent difference in fold amplitude calculation. The folded surface of each isolated fault is superposed to create an additive fold surface. The additive surface is subtracted from the interactive surface and divided by the maximum fold amplitude associated with an isolated fault to give a percent difference in amplitude.

distance between the faults show negligible fault interaction. For small and separated secondary faults of the geometry presented in Fig. 7D, the maximum change in uplift between the interactive and superposed fold models is only 1% of the maximum uplift (Table 1). Furthermore, the fold surface uplift differs by less than 5% between the interactive and superposed fold models for all variations of depth, strike, dip and contraction direction for secondary faults less than 50% than the size of the primary fault (Table 1). Because these fold patterns are not altered by fault interaction, the geometry of such faults could be independently inferred from each observed fold. However, as noted earlier, some of these fault configurations produce only one fold axis so that the second fault could be unrecognized.

Shallow faults may have greater interaction than deeper faults because the thinner superstrata facilitates deformation by providing less resistance to bending. For this reason, we examine the folded surface overlying 250-m-deep faults with separated secondary faults 50% the length of the primary and a maximum uplift difference of 3%. Although decreasing the depth by 75% produces a slight increase in the percent difference in uplift, the maximum difference is less than 5% and the effect of fault interaction is negligible.

5.2. Interacting fault configurations

For fold patterns that show a maximum uplift difference greater than 5%, we further explore fault interaction by mapping the difference in net slip between equivalent interacting and isolated faults. An isolated, elliptical fault with uniform traction in an elastic half-space has a symmetric slip pattern; highest slip occurs in the center and slip decreases towards the fault periphery (e.g. Lawn, 1975). Perturbations from this slip pattern reveal interactions between the faults (Willemse et al., 1996; Maerten et al., 2000). For example, areas with the greatest uplift difference should overlie areas along the faults that have the greatest redistribution of slip due to fault interaction. Consequently, the inference of fault geometry from individual folds in these areas would yield errors.

Two faults of the same size show evidence of fault interaction even when separated (Table 1). The fold surface overlying areas of the primary fault within the shadow of the secondary fault (south of intersection) has 8% less uplift in the interactive model, whereas the area outside the shadow has a maximum of 5% more uplift (Fig. 9B). Thus, superposing deformation associated with two separated and coeval faults under-predicts fold amplitude on the northern half and over-predicts on the southern half of the primary fault. The difference in uplift reflects differences in the distribution of slip between the interactive and superposed models (Fig. 9). Slip decreases along areas of the primary fault under the stress shadow of the secondary fault and increases along areas outside the shadow. Slip distribution along the secondary fault remains similar to the distribution along an isolated secondary fault.

Two equal-sized faults that touch or are mated have the greatest degree of fault interaction. Two faults of the same size and connected by one node display a distinctly asymmetric slip pattern along the abutted fault with lesser slip along the region within the stress shadow of the secondary fault and greater slip along the half that is not overlapped by the secondary fault (Fig. 10C). The difference in uplift reflects this slip partitioning; the folded surface of the interactive model is 12% lower than the superposed model above the overlapped primary fault and 5% greater above the half of the primary fault outside the shadow (Fig. 9C).

Mated models with secondary fault size at both 50 and 100% of the primary fault size show the greatest degree of fault interaction (Table 1). For both of these models, the abutted fault has a distinct partitioning of slip with the most slip occurring on the fault half not overlapped by the abutting fault (Figs. 9D and 10A). Due to this interaction, the secondary fault and the northern half of the primary act as one kinked fault. Because these two faults behave similarly to one thoroughgoing fault when mated, they produce a significant difference in uplift between the interactive and superposed models, with a maximum of 26% less uplift for the larger secondary fault and a 14% less uplift for the smaller secondary fault (Fig. 9A and D). The pattern of uplift difference remains the same for the smaller and larger mated faults and, as expected, the model with the larger mated secondary fault has greater uplift difference than the model with the secondary fault 50% of the primary

Fig. 9. Percent uplift difference between the interactive and superposed fold surfaces for fault pairs that show significant interaction. Faults are (A) difference sizes and mated, (B) the same size and separated, (C) the same size and connected, and (D) the same size and mated. Contour interval is 3%. Percent uplift difference increases as the distance between the faults decreases and subsequent fault interaction increases.

Fig. 10. View perpendicular to each fault surface of the difference in normalized net slip from that of an isolated fault for (A) mated faults of difference sizes, (B) separated 1 km, (C) connected, and (D) mated faults of the same size. Slip is normalized to the maximum slip of an isolated primary fault. Each fault dips 60° and the secondary fault strikes 45° from the primary fault. The contour interval is five units of normalized slip. Dashed lines indicate a decrease in slip magnitude from that of an isolated fault. Slip distribution on the primary fault is increasingly asymmetric with proximity of the secondary fault. Higher slip arises on the northern half of the primary fault, whereas slip along the secondary fault remains similar to the slip distribution along an isolated secondary fault.

fault size due to greater slip partitioning. With the mated faults, the superposed model overpredicts slip along the southern half of the primary fault.

Although the maximum difference in uplift between interactive and superposed models may be significant, the fold patterns may not be distinguishable on geologic or structure contour maps (Fig. 11). The resulting fold pattern for both the interactive and superposed models is an approximately triangular fold with a bifurcated southern termination. However, some features of the folds above mated faults vary between the models. The western leg (A on Fig. 11) extends slightly further south in the interactive model. Additionally, the interactive model has a welt on the northeast side of the primary fold, just east of where the two faults intersect (B on Fig. 11). These subtle differences are due to the slip partitioning along the primary fault. Net slip on the secondary fault is greater in the interactive model, thereby amplifying folding on the western limb.

5.3. Implications

The degree of fault interaction, as evidenced by the difference between uplift of a folded surface created by interacting faults and one created by superposing equivalent isolated faults, depends on fault geometry. Where the secondary fault is smaller than the primary, the faults do not interact unless they are mated. This lack of interaction benefits geologic studies because each fault may be considered isolated and their associated fold patterns superposed. Thus, the geometry of each fault could be inferred independently from each observed fold. Furthermore, two mated faults with a smaller secondary fault produce a single doubly-plunging anticline rather than multiple fold axes for separated faults (Fig. 7F). Thus, the presence of a small secondary fold implies the faults are not interacting and not mated. However, the presence of a large fold may indicate interacting equal-sized primary and secondary faults.

Although fault slip along mated non-equal sized faults may be asymmetrically distributed due to fault interaction, the resultant fold pattern such as is expressed on a geologic map, resembles folding by one isolated fault; this allows for the inference that only one fault created the pattern. Further insights into this interaction can be gained by examining slip patterns on these interacting faults in detail. Slip that would have been distributed along the southern half of the primary fault, in the shadow of the secondary, is now taken up by the secondary fault. Essentially, the secondary fault and the northern half of the primary fault act as one non-planar fault to produce one fold. Thus, when predicting subsurface fault shape from fold pattern, one might presume that only one non-planar fault was creating the fold pattern due to the kink in the fold axis (Shamir and Eyal, 1995); in terms of slip distribution, this assumption would be acceptable. However, the unrecognized southern half of the primary fault could be geologically significant. For example, in actively deforming regions, the southern half of the primary fault could increase slip rate under a shift in local stress field and become more favorably aligned for slip to the local contraction direction. If the fault was unrecognized, the seismic hazard of the region could be underestimated. Furthermore, faults in hydrocarbon reservoirs may serve as seals or flow conduits. Unrecognized faults, such as the southern half of the primary fault, could contribute to misinterpretation in flow properties of a reservoir.

Although equal sized fault pairs have asymmetric and

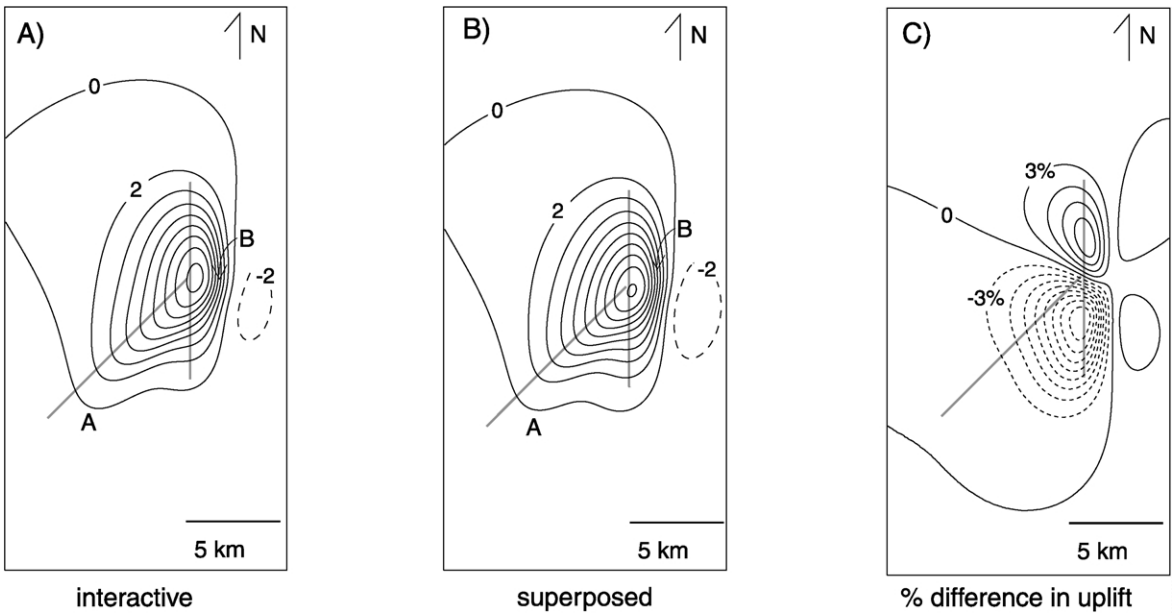

Fig. 11. Comparison of interactive (A) and superposed (B) fold surfaces for two mated faults of the same size. Contour interval for (A) and (B) is 2 m. Although the two surfaces differ, as indicated by the percent difference in uplift (C), visually the folds look similar. Contour interval for (C) is 3%. Consequently, fault geometry could be inferred from fold pattern by assuming that each fault folds the layer separately.

partitioned patterns of slip that produce multiple fold axes, the fold pattern as expressed on a geologic map or structure contour map due to interacting faults tested in this study is nearly indistinguishable from the superposed surface. However, these models are run at 1% far-field strain and the modeled folds have a maximum amplitude on the order of meters. If the percent difference in fold amplitude determined in this study holds for larger strains, the difference between fold surfaces could be hundreds of meters for strains of 100%. Such discrepancies between observed and modeled fold patterns may be noticeable in map pattern. For example, the discrepancies between interactive and superposed fold patterns pointed out on Fig. 11 could become more conspicuous upon further contraction of these faults. Thus triangular fold map patterns, such as the fold in Fig. 11, may overlie faults with significant interaction.

6. Conclusions

In order for multiple folds to form, faults must be similar in size, or the smaller fault must be shallower. Additionally, faults must be oblique or perpendicular to the principal contraction direction. Although multiple faults may be present in an area undergoing contraction, multiple faults do not produce multiple folds if these conditions are not met. A single fold does not constrain the presence of only one underlying fault surface, suggesting that fault surfaces could remain unrecognized if only fold patterns are used to constrain fault configuration. Faults do not interact unless they are either connected or equal in size and proximal. Significant slip partitioning indicates fault interaction and arises where the two faults are mated. At low strains, fault interaction can alter fold amplitudes compared with amplitudes of superposed isolated faults but has little observable effect on overall fold patterns.

Acknowledgements

This paper benefited greatly from reviews by Tom Blenkinsop, John Smith and Laurent Maerten. The work was supported by NSF grant EAR-9706548.

References

Allmendinger, R., Shaw, J., 2000. Estimation of fault propagation distance from fold shape; implications for earthquake hazard assessment. Geology 28 (12), 1099–1102.

Andrews, D., Pierce, W., Kirby, G., 1944. Structure contour map of the Big Horn Basin, Wyoming and Montana. U.S. Department of Interior Geological Survey.

Cashman, P.H., Ellis, M.A., 1994. Fault interaction may generate multiple slip vectors on a single fault surface. Geology 22 (12), 1123–1126.

Cooke, M., Pollard, D.D., 1997. Bedding-plane slip in initial stages of fault-related folding. Journal of Structural Geology 19, 567–581.

Crouch, S.L., Starfield, A.M., 1990. Boundary Element Methods in Solid Mechanics. Unwin Hyman, London.

Hennier, J., Spang, J., 1983. Mechanisms for deformation of sedimentary strata at Sheep Mountain Anticline, Big Horn Basin, Wyoming. Wyoming Geological Association Guidebook, 34th Annual Field Conference, pp. 97–111.

Johnson, K., Johnson, A., 2001. Mechanical analysis of the geometry of forced-folds. Journal of Structural Geology 24, 401–410.

Lawn, B., 1975. Fracture of Brittle Solids. Cambridge University Press, Cambridge.

Maerten, L., Willemse, E.J.M., Pollard, D.D., Rawnsley, K., 1999. Slip distributions on intersecting normal faults. Journal of Structural Geology 21, 259–271.

Mikumo, T., Singh, S.K., Santoyo, M.A., 1999. A possible stress interaction between large thrust and normal faulting earthquakes in the Mexican subduction zone. Bulletin of the Seismolgical Society of America 89 (6), 1418–1427.

Rowan, M.G., Linares, R., 2000. Fold-evolution matrices and axial-surfaces of fault-bend folds; application to the Medina Anticline, Eastern Cordillera, Columbia. AAPG Bulletin 84 (6), 741–764.

Savage, H., Cooke, M., 2003. Can flat-ramp-flat fault geometry be inferred from fold shape?: a comparison of kinematic and mechanical folds. Journal of Structural Geology, in press.

Shamir, G., Eyal, Y., 1995. Elastic modeling of fault-driven monoclinal fold patterns. Tectonophysics 245 (1-2), 13–24.

Smith, J.V., Marshall, B., 1992. Patterns of imbricate folding and fold interference in oblique contraction of layered rocks of the inverted Cobar Basin, Australia. Tectonophysics 215, 319–335.

Suppe, J., 1983. Geometry and kinematics of fault-bend folding. American Journal of Science 283 (7), 684–721.

Suppe, J., Medwedeff, D.A., 1990. Geometry and kinematics of fault-propagation folding. Eclogae Geologicae Helvetiae 83 (3), 409–454.

Thomas, A.L., 1994. POLY3D: a three-dimensional, polygonal element, displacement discontinuity boundary element computer program with applications to fractures, faults, and cavities in the Earth's crust. Unpublished Master's thesis, Stanford University.

Willemse, E.J.M., Pollard, D.D., Aydin, A., 1996. Three-dimensional analyses of slip distributions on normal fault arrays with consequences for fault scaling. Journal of Structural Geology 18 (2/3), 295–309.